Analysing the structure of the optical path length of a supersonic mixing layer by using wavelet methods*

Gao Qiong(高 穹)[a)†], Yi Shi-He(易仕和)[b)], Jiang Zong-Fu(姜宗福)[a)], Zhao Yu-Xin(赵玉新)[b)], and Xie Wen-Ke(谢文科)[a)]

[a)] *College of Photon–Electron Science and Engineering, National University of Defense Technology, Changsha* 410073, *China*
[b)] *College of Aerospace and Material Engineering, National University of Defense Technology, Changsha* 410073, *China*

(Received 17 October 2011; revised manuscript received 6 December 2011)

The nano-particle-based planar laser scattering (NPLS) technique is used to measure the density distribution in the supersonic mixing layer of the convective Mach number 0.12, and the optical path difference (OPL), which is quite crucial for the study of aero-optics, is obtained by post processing. Based on the high spatiotemporal resolutions of the NPLS, the structure of the OPL is analysed using wavelet methods. The coherent structures of the OPL are extracted using three methods, including the methods of thresholding the coefficients of the orthogonal wavelet transform and the wavelet packet transform, and preserving a number of wavelet packet coefficients with the largest amplitudes determined by the entropy dimension. Their performances are compared, and the method using the wavelet packet is the best. Based on the viewpoint of multifractals, we study the OPL by the wavelet transform maxima method (WTMM), and the result indicates that its scaling behaviour is evident.

Keywords: optical path difference, aero-optics, supersonic mixing layer, wavelet, coherent structures, scaling behavior

PACS: 47.40.Ki, 47.80.JK, 47.53.+n, 42.25.Dd **DOI:** 10.1088/1674-1056/21/6/064701

1. Introduction

The optical path length (OPL) or optical path difference (OPD) is the primary quantity for the study of aero-optics.[1,2] For airborne laser systems, the OPL can be used to calculate the far-field Strehl ratio, beam wander, beam spread, and other high order quantities,[3] which are important for measuring the beam quality. For airborne imaging systems, the optical transfer function due to the aero-optical aberrations can also be calculated with the relevant OPL,[4] and the imaging blurring and jitter can then be estimated. Another reason for the study of the OPL is to explore the flow information carried by it. The OPL due to the flow density can be defined as

$$L(x,y)=\int_{z_0}^{z_1} n'(x,y,z)\,\mathrm{d}z=\int_{z_0}^{z_1} K_{\mathrm{GD}}\rho(x,y,z)\,\mathrm{d}z, \tag{1}$$

where n' is the refractive index subtracted by 1, z is the direction of optical propagation, K_{GD} is the Gladstone–Dale constant, and ρ is the density of the flow. So the OPL is related directly to the density of the flow, and one may expect to investigate the flow structure from it.

Experiment is a basic tool for the study of OPL and aero-optics. From the traditional interferometric method to the Malley probe, the small-aperture beam technique and the high-bandwidth Hartmann sensor,[5–8] various techniques have been devised to directly measure the aberrated wave-front. Despite great progress in many aspects, the measurement of OPL with a high spatiotemporal resolution is still unavailable by using these methods, especially for supersonic flow with high spatial and temporal frequencies. Fortunately, with the introduction of the flow field visualization technique, measurements of this kind are becoming available. Dimotakis *et al.*[9] obtained the refractive index fields of shear layers and jets by the Rayleigh scattering of a thin sheet laser by binary-mixture components. Zubair and Catrakis[10] measured the refractive index fields of separated shear layers by laser-induced fluorescence.

Numerical simulation is another important method to assess the OPL of turbulent flow. Tru-

*Projected supported by the Innovation Research Foundations for Postgraduates of National University of Defense Technology and Hunan Province, and the National Natural Science Foundation of China (Grant No. 61008037).

†Corresponding author. E-mail: gaoqiong1980@126.com

© 2012 Chinese Physical Society and IOP Publishing Ltd

man and Lee[11] performed the direct numerical simulation (DNS) of a turbulent shear flow, and studied the coherent structures on the optical beam propagation. Recently Mani *et al.*[12] solved the high Reynolds number flow over a circular cylinder by large eddy simulation (LES), and the far-field optical statistics under many configurations are obtained. In addition, Fitzgerald and Jumper[13] used the vortex method to study the optical distortion of a nearly incompressible mixing layer.

In recent years, our group[14−17] has developed the nano-particle-based planar laser scattering technique (NPLS), which has been used successfully to measure the density field and the velocity field of the supersonic flow around a body and the supersonic mixing layer. Due to its high spatiotemporal resolutions, the fine flow field structure and its temporal evolution can be observed clearly. Thus, this technique can offer great convenience for the study of aero-optics. The OPL of a supersonic mixing layer obtained by using the NPLS technique has been studied from the viewpoints of correlation function and structure function.[18]

The purpose of the present paper is to analyse the OPL by wavelets. The rest of the present paper is organized as follows. In Section 2, we present the relevant theory of wavelet transform (WT) and the wavelet transform maxima method (WTMM) for multifractal analysis, which are basic tools of the present study. In Section 3, a brief description of the experimental setup is given, including the designs of the supersonic layer wind tunnel and the NPLS system, and the measured density distribution and the calculated OPL are also presented. In Section 4 the problem of extracting the coherent structures of the OPL is studied, and analysed from the viewpoint of multifractals. Finally in Section 5 some conclusions are drawn from the present study.

2. Theories of wavelet analysis and the WTMM method

2.1. Wavelet analysis

Wavelet methods have been introduced to analyse, model, and compute turbulent flows.[19−25] There are two kinds of wavelet transforms: the continuous wavelet transform (CWT) and the orthogonal wavelet transform (OWT). We refer the reader to Refs. [26] and [27] for the complete theory and more wavelet applications. For the purpose of this paper, we briefly introduce the one-dimensional (1D) wavelet analysis.

For a mother wavelet ψ satisfying the admissible condition, we can generate a family of functions by translation and dilation

$$\psi_{r,x}(x') = r^{-1/2}\psi((x'-x)/r),\ r>0,\ x\in R. \quad (2)$$

With Eq. (2), the CWT of a 1D signal $s(x)$ is defined as

$$\hat{s}(r,x) = \int s(x')\bar{\psi}_{r,x}(x')\,\mathrm{d}x'. \quad (3)$$

The continuous values of r and x reflect the redundancy of CWT coefficients. The widely used wavelet for the CWT is the derivative of the Gaussian function, whose Fourier transform is

$$\tilde{\psi}(k) = k^p \exp(-k^2/2),\ p=2,4,\ldots. \quad (4)$$

The OWT relies on sampling $\psi_{r,x}$ in a discrete way

$$\psi_{ji}(x) = 2^{j/2}\psi(2^j x - i),\ j,i\in Z, \quad (5)$$

and this family of functions constitute an orthogonal basis of the space

$$\boldsymbol{W}_j = \mathrm{span}\{\psi_{ji}\}_{i\in Z}. \quad (6)$$

The OWT of a signal $s(x)$ can be expressed as the composition of its projection on $\boldsymbol{W}_j$

$$s(x) = \sum_{j=0}^{J-1}\sum_{i=0}^{2^j-1}\hat{s}_{ji}\psi_{ji}(x),\ \hat{s}_{ji} = \int s(x)\bar{\psi}_{ji}(x)\,\mathrm{d}x. \quad (7)$$

The wavelet packet (WP) generalizes the OWT by dividing the frequency axis uniformly. The basic idea is splitting the vector space recursively to obtain a binary tree. The WP offers great flexibility in choosing a proper basis according to a particular requirement. In practice, one selects the "best" by minimizing a concave cost function, and we use the function $\Phi\ (x) = x^{1/2}$ in this paper.

The computations of CWT, OWT, and WP and the best basis selection in this paper are implemented by using the programs in WaveLab developed by Donoho.[28]

2.2. WTMM method

Fractal and multifractal concepts are important tools for turbulence, and have been widely used to study energy dissipation, velocity signal, mixing interface, and other important objects.[29−31] The basic idea is to characterize an object by the fractal dimension, or generally by a singularity spectrum.[32] The method of decomposing a singular measure into interwoven sets of singularity strength α, with dimension

$f(\alpha)$, has turned into a useful and compact way of describing the scaling behaviour of such a measure. The WTMM method[33−35] is a famous and successful technique for computing the spectrum $(\alpha,\ f(\alpha))$, and has achieved almost the status of standard.[36]

The WTMM method consists of building a partition function from the modulus maxima of the CWT, as

$$Z(q,r)=\sum_{l\in L(r)}\left[\sup_{(x,r')\in l}|\hat{s}(x,r')|\right]^q\sim r^{\tau(q)},\ q\in R, \quad (8)$$

where $L(r)$ denotes the set of all the maxima lines, and its exact definition can be found in the references cited above. With the scaling exponent $\tau(q)$, the singularity spectrum of function $s(x)$ an be determined from the Legendre transform as

$$\alpha(q)=\partial\tau(q)/\partial q,\ f(\alpha)=\min_q[q\alpha-\tau(q)]. \quad (9)$$

Provided that the vanishing moment of the wavelet is large enough, the correct singularity spectrum can be obtained. In practice the parameter q cannot be an arbitrary real value, and must be in within an appropriate range. Gao *et al.*[37] have proposed a technique to determine the range of q by checking whether the expressions

$$\mathrm{d}f(\alpha(q))/\mathrm{d}q=q,\ \partial^2\tau(q)/\partial q^2\leq 0 \quad (10)$$

can be fulfilled. Consult Ref. [32] for more details about Eq. (10).

3. Experiment

The experimental apparatus in this study mainly comprises the supersonic mixing layer wind tunnel and the NPLS system. The sketch of the apparatus is shown in Fig. 1, and a photograph of the whole system is shown in Fig. 2.

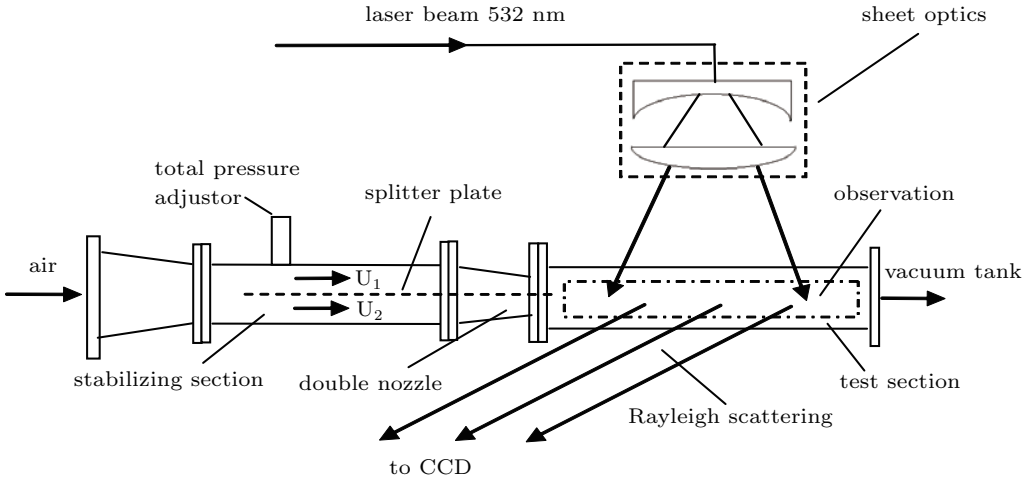


Fig. 1. Sketch of the experimental setup used in the present study. The main components are the supersonic mixing layer wind tunnel and the NPLS system. Find more detail in the text.

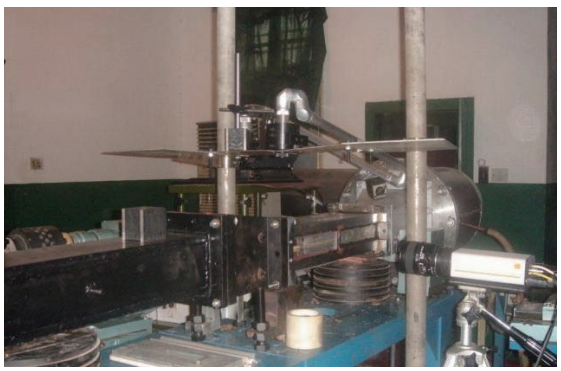


Fig. 2. (colour online) Photograph of the whole experimental system, including the supersonic mixing layer wind tunnel and the NPLS system.

Due to the existence of many kinds of instability mechanisms and shock waves in the supersonic compressible fluid, the design of supersonic mixing layer wind tunnel is very difficult. In recent years, Yi *et al.*[14] and Zhao[15] have successfully designed supersonic mixing layer wind tunnels, in which the shock wave can be excluded, and the whole evolution process of the mixing layer from initial instability to a developed vortex can be observed. This wind tunnel is composed mainly of a stabilizing section, a double nozzle, a test section, and other auxiliary equipment (including a butterfly valve, a total pressure adjuster, vacuum facility, etc.). The inflow is air pro-

cessed by using a desiccator, a dust catcher, and an air conditioner. The total pressure can be adjusted to realize pressure matching between the two streams. The double-nozzle contour is designed by using the B-spline curve method, which can provide uniform and low noise flow. Also, correction due to the boundary layer is necessary for the design of the nozzle. There are two aspects of the correction, including the influence of the thickness of the layer on the area of the cross section, and the interaction between the wave and the mixing layer. In practice, once the first aspect is corrected properly, the second can be restrained to some extent. The maximum runtime of this wind tunnel is about two minutes, and three convective Mach numbers (M_c) can be achieved as

$$M_c = (U_2 - U_1)/(a_1 + a_2) = 0.12, 0.24, 0.50,$$

where a_i and $U_i\,(i = 1, 2)$ are the sound velocity and the mean speed of the two streams. For lower M_c, the mixing layer can be considered approximately as a two-dimensional (2D) flow field. The case studied in this paper is of $M_c = 0.12$, and the relevant calibration parameters are shown in Table 1.

Table 1. Calibration parameters of the supersonic mixing layer wind tunnel with $M_c = 0.12$.

Property	Stream 1	Stream 2
Ma	2.884	3.649
P/Pa	1077.1	1077.1
$\rho/(\mathrm{kg/m^3})$	0.033	0.046
$U/(\mathrm{m/s})$	619.3	668.1

Another crucial component of the experiment is the NPLS system. The setup is composed of a tracer generation system, a light source system, a recording system, a synchronization system and a post-processing system. TiO_2 particles with diameters at nanometer scale (18 nm) are selected as tracers in the NPLS system, and an experiment where shock waves are passed through it indicates that TiO_2 particles can follow the supersonic flow faithfully. The tracer particles are assumed to be spherical, and their scattering character is related to scattering angle, incident laser wavelength, diameter, etc., which can be expressed by using the Rayleigh scattering theory. When the scattering angle is 90° and the polarization direction is perpendicular to the scattering plane, flow images with high signal noise ratio can be captured by CCD. The light source is a dual-cavity Nd:Yag laser (wavelength 532 nm, pulse width 6 ns, energy per pulse 350 mJ). A very thin laser sheet is generated by the sheet optics system, and then illuminates the flow region of interest. The recording system is an interline transfer CCD whose resolution is 2048×2048 and the shortest time interval of double-exposure can reach 0.2 μs by using the inter- frame technique. The synchronizer can adjust the laser emission and CCD exposure to make sure that the two laser pulses are exactly captured by the double exposures, respectively. How to mix the tracers into air uniformly and how to prevent the nanoparticles from aggregating into clusters of larger size are the two primary problems associated with the NPLS technique. We address the first issue by keeping constant pressure for the tracer generator and offering a stabilizing section with enough length for a wind tunnel, and address the second issue by fluidizing the tracers with a supersonic nozzle and using a cyclone separating device. According to the particle dynamics in multiphase fluid, we have measured the diameter of tracer particles in the NPLS system by using an oblique shock wave experiment.[16] The results give a diameter of about 40 nm, which indicates that the aggregating effect is surmounted effectively.

Figure 3 shows two time-correlated NPLS images obtained by this experimental apparatus. The exposure time is 5 ns, and the time interval between the two exposures is 5 μs. The size of the two images is 216×1500, and the width of the images is 240 mm, so the spatial resolution is $\delta = 0.16$ mm. From these images, one can observe the coherent structures clearly, and the temporal evolution can also be checked. Because the optical intensity along the streamwise direction is not uniform, image correction is necessary. This can be performed on the reasonable assumption that the density along the upper or lower part is uniform. For example, we can select a narrow region with a size of 8×1500 at the top part of the image, and divide it into small segments each with a size of 8×10. Taking the averaged pixel value of each segment as the measurement of optical intensity in this small region, we can correct it easily. With the corrected image and the calibration parameters in Table 1, we can calculate the density distribution easily, and then the OPL based on Eq. (1), which is shown in Fig. 3 under each NPLS image.

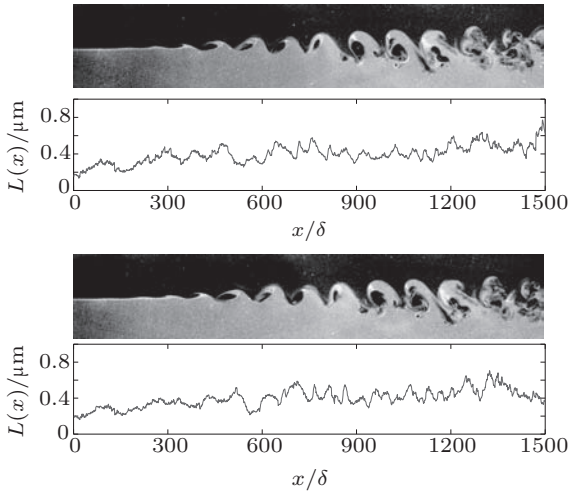


Fig. 3. Two time-correlated NPLS images and their OPLs of a supersonic mixing layer with $M_c = 0.12$ with the exposure time being 5 ns, and the time interval between the two exposures being 5 μs.

4. Structure of the OPL

One can find from the NPLS images in Fig. 3 that large-scale vortices dominate the flow, so we expect that there is relevant coherent structure for the OPL. The extraction of large-scale structures or coherent structures is a very important problem for turbulence research. There is not yet a universal definition for the coherent structures observed in turbulent flow. Here we adopt the idea in Refs. [21]–[24], i.e., turbulent flow is a superposition of coherent structures which is not Gaussian and has a random background that can be modeled by using Gaussian statistics. So the coherent structures can be obtained by subtracting a Gaussian background from the flow. Their method of extracting the coherent structures relies on thresholding the coefficients of the OWT, which is similar to the wavelet de-noising in signal processing. The estimation of a proper threshold is crucial for its application. Azzalini *et al.*[38] presented a recursive algorithm to determine the threshold, which is well suited for signals with a Gaussian background.

We use this method to analyse the OPL in Fig. 3, but the results (given in below) indicate that this method does not perform well. When thresholding WP coefficients calculated with the best basis, we can obtain quite good results. Now we describe this technique in detail.

Step 1 Select the best basis according to the cost function $\Phi(x) = x^{1/2}$, and compute the WP coefficients in this basis. Then estimate the variance initially as

$$\sigma^2 = (1/N)\sum\nolimits_i (L(x_i))^2 \tag{11}$$

and the threshold as $\varepsilon = \sqrt{2\sigma^2 \ln N}$, where N is the length of the OPL.

Step 2 Threshold the WP coefficients as

$$\hat{L}_{ji}^{\varepsilon} = \begin{cases} \hat{L}_{ji}, \text{ if } |\hat{L}_{ji}| \le \varepsilon, \\ 0, \text{ else}, \end{cases} \tag{12}$$

and count the number of the coefficients less than this threshold N^{ε}.

Step 3 Perform the inverse WP with the coefficients in Eq. (12) and the best basis to obtain L^{ε}. Then compute a new estimate for the variance as

$$\sigma^2 = (1/N)\sum\nolimits_i (L^{\varepsilon}(x_i))^2. \tag{13}$$

Return to Step 2 with this variance, and repeat the loop until the number N^{ε} does not vary.

Step 4 Obtain the large-scale structure by $L^C = L - L^{\varepsilon}$.

In addition to the methods based on OWT and WP, we also attempt Ruppert-Felsot *et al.*'s idea[39] by selecting N_e WP coefficients with the largest amplitude, where N_e is the entropy dimension (ED) defined as

$$N_e(L) = \exp(H(L)),\ H(L) = -\sum\nolimits_i p_i \ln p_i, \tag{14}$$

where

$$p_i = |L_i|^2/||L||^2,\ ||L||^2 = \sum\nolimits_i |L_i|^2. \tag{15}$$

For the convenience of description, we refer to these three methods as OWT, WP, and ED to avoid confusion.

Now we use these techniques to extract the coherent structures of the OPL in Fig. 3(b). Because the length of the analysed signal should be a power of 2, we choose the right part of the OPL with length 1024. The large scale structures obtained by using these three methods are shown in Fig. 4, and the statistics of the background are listed in Table 2. The used wavelet is Battle5 and the depth of the dyadic tree is 8. It can be found from Fig. 4 that the coherent structures obtained by OWT and WP are almost indistinguishable from the original OPL, but that the ED method only gives a basic profile. This can be explained by the compression ratio in Table 2. The number of retained coefficients is too small for the ED method, and much information has been lost. The other two methods can

reconstruct great details with quite a small number of coefficients, especially the WP method. Furthermore, the flatness and the skewness of the background obtained by the WP method deviate from 3 and 0 (too little), respectively, and the moments of the odd orders are negligible. So the background obtained in this way is closer to Gaussian distribution than the other two, thus it is more consistent with the statistical conjecture about the incoherent part. Our results indicate that the original OPL can be reconstructed with quite a few WP coefficients, thus OPL research can be converted into WP coefficient research. The functions in the wavelet basis relevant to WP coefficients with large amplitude can be considered as the coherent structures of OPL, which is represented more naturally in this way. Especially when the temporal evolution is concerned, investigating the evolution of WP coefficients with larger amplitudes is a more convenient way. In fact, a low-dimensional model for OPL can be constructed with the temporal evolution of WP coefficients with large amplitude.

In addition, it is surprising for the ED method that the background computed by this method obeys the Gaussian distribution quite well, despite that only 5 WP coefficients are used to represent the coherent structures. This result indicates that Farge *et al.*'s idea for extracting coherent structures is not fully rigorous. As mentioned earlier, there is not a strict definition for coherent structures, so their extraction method often has to be used in combination with other methods or some experience.

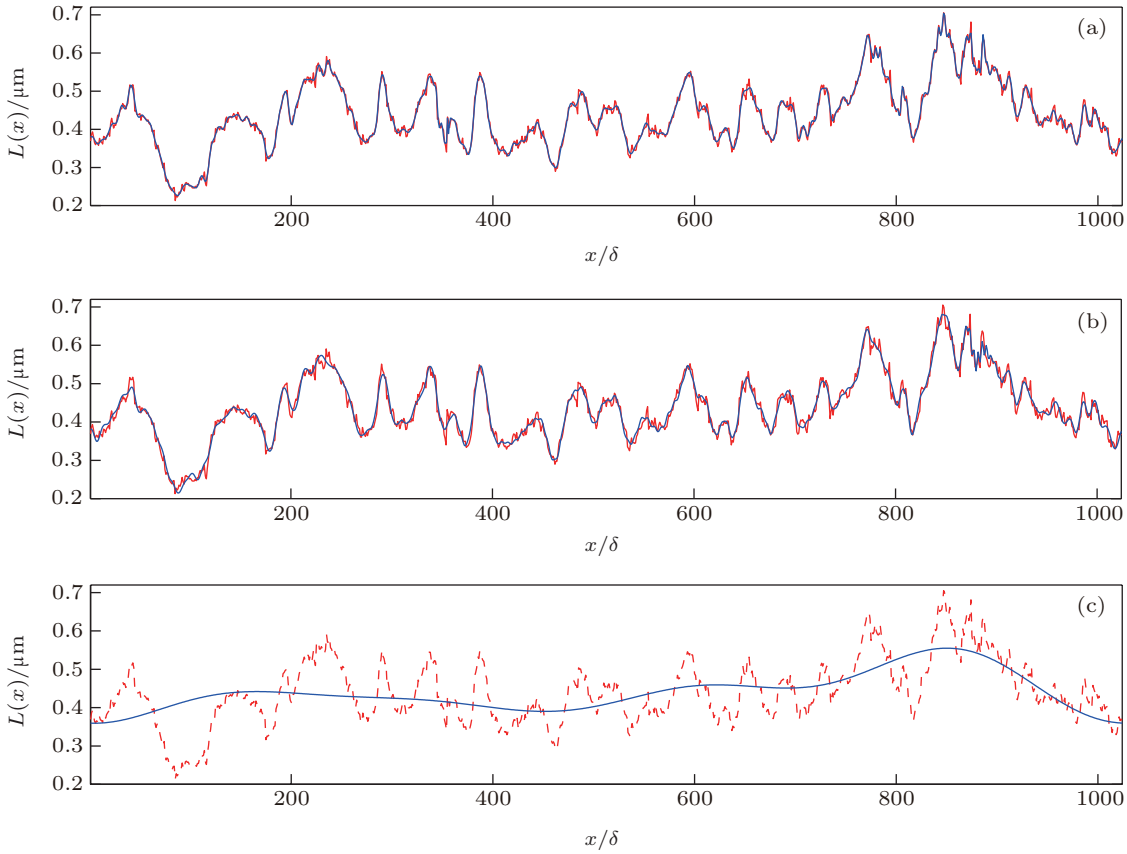


Fig. 4. (colour online) Coherent structures of the OPL (solid blue lines) extracted by the methods of (a) OWT, (b) WP, and (c) ED. The original OPL (dashed red line) is also shown in each panel for comparison.

Table 2. Statistics of the background of OPL obtained by the three methods.

Method	Compression ratio	Flatness	Skewness	M_3	M_5	M_7
OWT	1024/265	4.0	0.08	-6.8×10^{-8}	7.7×10^{-11}	1.5×10^{-13}
WP	1024/80	3.2	0.09	-2.4×10^{-7}	-4.6×10^{-10}	-7.6×10^{-13}
ED	1024/5	3.1	0.25	-7.8×10^{-5}	-3.6×10^{-6}	-1.2×10^{-7}

From the NPLS images in Fig. 3, we can find small vortices included by large ones, and this phenomenon is more evident for downstream flows. So we speculate the existence of self-similar structures, and the concepts of fractal and multifractals may be applicable, although the flow under study is not strictly fully developed. To confirm this speculation, we perform multifractal analysis of the OPL in Fig. 3(b) (right part with length 1024) by using the WTMM method. Our results indicate very obvious scaling behaviour over quite a large range of scale, and the scaling exponent and the singularity spectrum are shown in Fig. 5. In the computation the wavelet in Eq. (4) with $p = 4$ is used, and the range of parameter q determined by Eq. (10) is $[-2.7, 10]$ with interval $\Delta q = 1/10$. The α corresponding to the peak of the spectrum is about 0.3, and $f(1)$ is about 0.3. Also, there is a small part of the spectrum line with negative α. These results indicate quantitatively that the OPL is rather irregular.

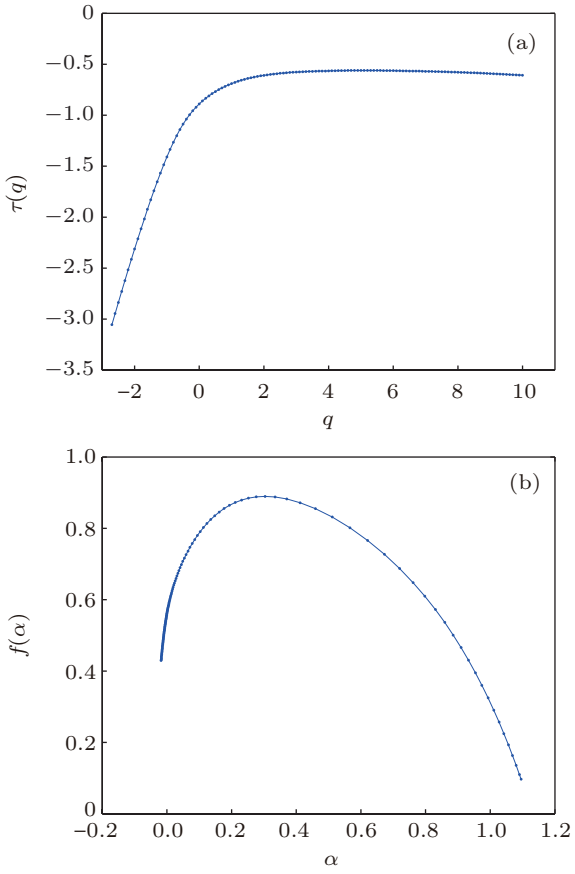


Fig. 5. Multifractal analyses of the OPL in Fig. 3(b) by using the WTMM method: (a) scaling function and (b) singularity spectrum.

5. Conclusion

In summary, in the present work, the OPL of a supersonic mixing layer is measured by using the NPLS technique, and its structure is analysed with the wavelet tool. With an inter-frame CCD and a double-cavity pulsed laser, the supersonic flow can be visualized with high spatiotemporal resolutions, and its OPL is computed through proper correction of the image. The OPL is due mainly to the coherent structures in the flow, and we expect the existence of relevant coherent structures in OPL. Three methods based on wavelets are used to extract the coherent structures of OPL, which are thresholding the coefficients of OWT and WP, and preserving a number of WP coefficients with largest amplitudes determined by the ED. The results, measured by the compression ratio and the background statistics, indicate that the WP method performs better than the OWT method. Also, the flow images suggest the possible existence of self-similar structures for OPL. The WTMM method is used to analyse OPL in this aspect, and its singularity spectrum is computed. The results validate our conjecture, and the scaling behaviour of OPL is quite evident.

References

[1] Gilbert K G and Otten L J 1982 *Aero-Optical Phenomena* (New York: AIAA)
[2] Jumper E J and Fitzgerald E J 2001 *Prog. Aerospace. Sci.* **37** 299
[3] Mani A, Wang M and Moin P 2006 *J. Opt. Soc. Am.* A **23** 3027
[4] Goodman J W 1996 *Introduction to Fourier Optics* (New York: McGraw-Hill)
[5] Trolinger J D 1982 "Aero-optical characterization of aircraft optical turrets by holography, interferometry and shadowgraph." in Gilbert K G and Otten L J (ed.) *Aero-Optical Phenomena* (New York: AIAA) p. 200
[6] Malley M, Sutton G W and Kincheloe N 1992 *Appl. Opt.* **31** 4440
[7] Hugo R J and Jumper E J 1996 *Appl. Opt.* **35** 4436
[8] Abado S, Gordeyev S and Jumper E J 2009 *Proc. SPIE* **7466** 746602
[9] Dimotakis P E, Catrakis H J and Fourguette D C 2001 *J. Fluid Mech.* **433** 105
[10] Zubair F R and Catrakis H J 2007 *AIAA J.* **45** 1663
[11] Truman C R and Lee M J 1990 *Phys. Fluids* A **2** 851
[12] Mani A, Moin P and Wang M 2009 *J. Fluid Mech.* **625** 273
[13] Fitzgerald E J and Jumper E J 2004 *J. Fluid Mech.* **512** 153
[14] Yi S H, Zhao Y X, He L, Cheng Z Y and Tian L F 2007 *Chin. Conf. Theor. Appl. Mech.* p. 190

[15] Zhao Y X 2008 "Experimental study of the spatiotemporal structure of supersonic mixing layer" Ph. D Dissertation Changsha, National University of Defense Technology (in Chinese)
[16] Zhao Y X, Yi S H, Tian L F and Cheng Z Y 2009 *Sci. Chin.* E **52** 3640
[17] Tian L F, Yi S H, Zhao Y X, He L and Cheng Z Y 2009 *Sci. Chin.* G **52** 1357
[18] Gao Q, Jiang Z F, Yi S H and Zhao Y X 2010 *Appl. Opt.* **49** 3786
[19] Meneveau C 1991 *J. Fluid Mech.* **232** 469
[20] Farge M 1992 *Ann. Rev. Fluid Mech.* **24** 395
[21] Farge M 1999 *Phys. Fluids* A **11** 2187
[22] Farge M 2001 *Phys. Rev. Lett.* **87** 054501
[23] Farge M, Schneider K, Pellegrino G, Wray A A and Rogallo R S 2003 *Phys. Fluids* A **15** 2886
[24] Ruppert-Felsot J, Farge M and Petitjeans P 2007 *J. Fluid Mech.* **636** 427
[25] Schneider K and Vasilyev O V 2010 *Ann. Rev. Fluid Mech.* **42** 473
[26] Daubechies I 1992 *Ten Lectures on Wavelets* (Philadelphia: SIAM)
[27] Mallat S. A 2003 *Wavelet Tour of Signal Processing* (Singapore: Elsevier)
[28] Donoho D Wavelab http://www-stat.stanford.edu/∼wavelab
[29] Mandelbrot B 1974 *J. Fluid Mech.* **62** 331
[30] Meneveau C and Sreenivasan K R 1991 *J. Fluid Mech.* **224** 429
[31] Sreenivasan K R 1991 *Ann. Rev. Fluid Mech.* **23** 539
[32] Halsey T C, Jensen M H, Kadanoff L P, Procaccia I and Shraiman B I 1986 *Phys. Rev.* A **33** 1141
[33] Muzy J F, Bacry E and Arneodo A 1991 *Phys. Rev. Lett.* **67** 3515
[34] Muzy J F, Bacry E and Arneodo A 1993 *Phys. Rev.* E **47** 875
[35] Arneodo A, Bacry E and Muzy J F 1995 *Physica* A **213** 232
[36] Audit B, Bacry E, Muzy J F and Arneodo 2002 *IEEE Trans. Inform. Theor.* **48** 2938
[37] Gao Q, Liao T H and Cui Y F 2008 *Chin. Phys.* B **17** 2018
[38] Azzalini A, Farge M and Schneider K 2005 *Appl. Comput. Harmon. Anal.* **18** 177
[39] Ruppert-Felsot J E, Praud O, Sharon E and Swinney H L 2005 *Phys. Rev.* E **72** 016311